Phys Chem Minerals (1999) 26: 576–583

ORIGINAL PAPER

E. Huang · J.-F. Lin · J. Xu · T. Huang
Y.-C. Jean · H.-S. Sheu

Compression studies of gibbsite and its high-pressure polymorph

Received: 28 September 1998 / Revised, accepted: 22 December 1998

Abstract Various X-ray diffraction methods have been applied to study the compression behavior of gibbsite, $Al(OH)_3$, in diamond cells at room temperature. A phase transformation was found to take place above 3 GPa where gibbsite started to convert to its high-pressure polymorph. The high-pressure (HP) phase is quenchable and coexists with gibbsite at the ambient conditions after being unloaded. This HP phase was identified as nordstrandite based on the diffraction patterns obtained at room pressure by angle dispersive and energy dispersive methods. On the basis of this structural interpretation, the bulk modulus of the two polymorphs, i.e., gibbsite and nordstrandite, could be determined as 85 ± 5 and 70 ± 5 GPa, respectively, by fitting a Birch-Murnaghan equation to the compression data, assuming their K'_o as 4. Molar volume cross-over occurs at 2 GPa, above which the molar volume of nordstrandite is smaller than that of gibbsite. The differences in the molar volume and structure between the two polymorphs are not significant, which accounts for the irreversibility of the phase transition. In gibbsite, the axial compressibility behaves as $c/c_o > a/a_o > b/b_o$. This is due to the fact that the dioctahedral sheets along the *c*-axis are held by the relatively weak hydrogen bonding, which results in the greater compressibility along this direction. In nordstrandite, the axial compressibility is $b/b_o > c/c_o > a/a_o$, which can also be interpreted as resulting from the the existence of hydrogen bonds along the *b*-axis.

E. Huang (✉) · J. Xu · T. Huang
Institute of Earth Sciences, Academia Sinica,
P.O. Box 1-55, Nankang, Taipei, Taiwan, R.O.C.

J.-F. Lin
Geophysical Science, University of Chicago,
Chicago, IL., U.S.A.

Y.-C. Jean · H.-S. Sheu
Synchrotron Radiation Research Center,
Hsinchu, Taiwan, R.O.C.

Introduction

The water reservoir in the Earth's mantle may be dominately hosted in the hydrous minerals (e.g., Akimoto and Akaogi 1984). Therefore, the study of hydrous minerals at high-pressure and temperature is crucial for understanding the dynamic processes of water circulation in the mantle. Examples such as triggering deep focus earthquakes (Kirby 1987; Meade and Jeanloz 1991) and regulating the water budget have been documented in hydrous minerals under mantle environments. In the past few years, some hydrous minerals with trioctahedral layer structure such as brucite ($Mg(OH)_2$) (e.g., Duffy et al. 1995; Xia et al. 1998) and portlandite ($Ca(OH)_2$) (Desgranges et al. 1993; Pavese et al. 1997) have been studied by the high-pressure experiments from which important geophysical implications are documented. These hydrous minerals show different behaviors at high pressures, such as amorphization in $Ca(OH)_2$ (Meade and Jeanloz 1990) and dehydration in $Mg(OH)_2$ (Johnson and Walker 1993). In our previous works, we have devoted ourselves to the studies of the high-pressure behaviors of hydrous and anhydrous aluminum oxides (Huang et al. 1995; Xu et al. 1995; Huang et al. 1996). Some of these compounds, such as diaspore, AlO(OH), do not show a significant change in structure but yield unexpected variations in Raman modes at high pressures (Huang et al. 1995). On the other hand, gibbsite, $Al(OH)_3$, shows drastic changes in both Raman and diffraction patterns at high pressures (Huang et al. 1996). The results obtained from the Raman spectroscopic studies are of interest when compared with those of other OH-bearing minerals at high pressure (Kruger et al. 1989). Therefore, it is obvious that more high-pressure research on compounds in the Al_2O_3-H_2O system should be conducted in order to understand the behavior of the OH-bearing phases and the phase relationships of minerals in the system.

Gibbsite with a space group of $P2_1/n$ has an analogous structure as brucite but possesses dioctahedral

layers in contrast to those trioctahedral layers in magnesian hydrous phases. Huang et al. (1996) reported that gibbsite undergoes a polymorphic phase transition above 3 GPa based on Raman and X-ray observations. The high-pressure phase was tentatively determined to be nordstrandite (space group $P1$) based on the diffraction patterns of the sample yielded from the unloading process. Unfortunately, their high-pressure X-ray data were inadequate to justify whether this high-pressure phase is indeed nordstrandite. Therefore, we have carried out further in situ high-pressure study on gibbsite and also a more detailed structural identification of the high-pressure phase. Furthermore, the compressibility can be determined for the two phases.

Energy dispersive X-ray diffraction (EDXRD) has routinely been used as a tool in the study of materials under pressures with synchrotron X-ray radiation. Recently, much progress has been made in the detecting system of the angle dispersive X-ray diffraction (ADXRD) method. Among all the detectors used in the ADXRD method, the image plate (IP) has proven to be the most efficient way for the collection of the diffraction signals. IP is a photosimulatable fluorescent plate, which is a digitally readable X-ray photograph. It has the characteristics of high absorption coefficient, sensitivity and greater dynamic range than the conventional ADXRD detectors and it also has the capability of being easily read out (Shimomura et al. 1992). Hence, IP has proven to be a very efficient detector for the angle dispersive X-ray diffraction in diamond anvil cell (DAC) experiment (Huang 1996). Moreover, the data can be digitized for structural analysis, which makes this method suitable for high-pressure diffraction research especially when synchrotron radiation is used (Chen and Takemura 1993). The application of IP to the X-ray studies and structural refinement of samples in diamond anvil cells were successfully carried out by Shimomura et al. (1992) and Nelmes et al. (1992). In this report, we will demonstrate the use of EDXRD and ADXRD methods in studying the pressure-induced phase transition in $Al(OH)_3$ at room temperature.

Experimental methods

The Baker Company's product of synthetic gibbsite powder, which was the same sample used by Huang et al. (1996), was used as the starting material for all experiments in this study. Both EDXRD and ADXRD methods were used to study the compression of gibbsite at room temperature. The experimental set up is described below.

ADXRD method

Two different ADXRD methods were used in this study. Their main goal is to examine the gibbsite sample that was quenched to the ambient conditions after it was compressed beyond the transition pressure. The two ADXRD methods differ in the X-ray source and the detector used for the collection of the diffraction signal.

In the first method, gibbsite powder was confined by a stainless steel gasket and then compressed in a diamond cell up to a nominal pressure of 5 GPa. The sample was then unloaded and mounted on a sample holder in a Debye-Scherrer camera (with a diameter of 57.3 mm) in which a photographic film was inserted. The X-ray source used was CoKα radiation with running conditions of 45 KV and 30 mA. It took 24 hours for the exposure of the film to collect the diffraction signal.

In the second method, the image plate (IP) was used in coupled with the synchrotron radiation of the Synchrotron Radiation Research Center (SRRC), Hsin-Chu, Taiwan. A monochromatic beam of 14.5 KeV was used as the X-ray source. The sample was loaded in the hole (250 μm diameter) of a gasket made of stainless steel and then slightly compressed between the diamond anvil cell so as to fill up the sample chamber. The cell was then mounted and aligned to bring the collimated X-ray beam (normally of the order of 100 μm) to fall on the sample in the diamond cell. The sample was then compressed to approximately 6 GPa and quenched to room pressure. The diffraction patterns of the sample at high-pressure and quenched condition were collected by the image plate with an exposure time of 24 hours. Optical alignment using a monitor that traced the image of the sample ensured that the position of the sample did not change during the process of removing and remounting of the sample.

EDXRD method

Two sets of runs were conducted in the EDXRD experiments. One was to identify the quenched phase and to correlate with the results obtained by the ADXRD method. The other was to determine the compressibility of the two polymorphs of $Al(OH)_3$. The white radiation component of synchrotron radiation was used as the X-ray source for both runs.

In the quenching experiment, the gibbsite sample was loaded in the gasket hole of a stainless steel and compressed in a diamond cell above the phase transition pressure. Several diffraction patterns were taken to monitor the process of the transition. The pressure was then decreased to the ambient conditions and the diffraction pattern of the quenched phase was taken. No pressure calibrant was loaded in the cell because the run was designed to take the diffraction pattern of the quenched phase without interfering peaks from pressure calibrant. The run was carried out at the B2 station of Cornell High Energy Synchrotron Source, Cornell University. Except for the 2θ angle (taken at 14°), the experimental geometry and data acquisition time are similar to those of the compressibility run described below.

In the compressibility run, the sample was mechanically mixed with gold powder and loaded in a diamond anvil cell. A T301 stainless steel was used as the gasket with a diameter of 200 μm for the sample chamber. Methanol-ethanol (4:1) solution was used as pressure medium to maintain a hydrostatic condition. The experiments were conducted at beamline X-17C, National Synchrontron Light Source, Brookhaven National Laboratory. An energy dispersive X-ray diffraction pattern was taken each time after the pressure increment was made. An intrinsic Ge detector was set at an angle (2θ) of 7° and the acquisition time for each spectrum was about 10 minutes. The X-ray beam size was limited to 30×30 μm. Gold was used as pressure calibrant (Heinz and Jeanloz 1984) and the average error in pressure measurements was ± 0.3 GPa. All of the spectra were treated by Jandel Scientific Peak-Fit Program for the position of diffraction peaks.

Results

Quenched phase

Figure 1 shows the diffraction patterns of the quenched product obtained by the methods using film, image plate and Ge-detector as recording systems. The diffraction pattern obtained by the photographic film is shown in

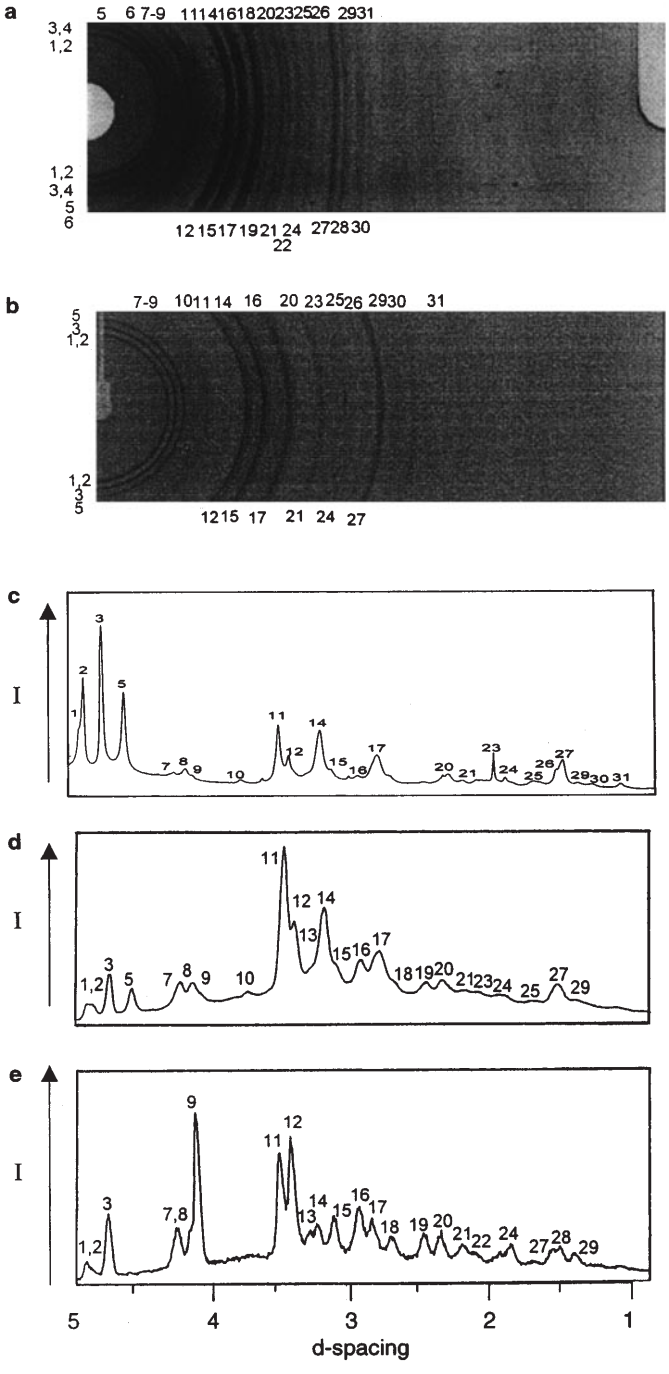

Fig. 1a–e The diffraction patterns of quenched sample obtained by **a** film **b** image plate and **d** EDXRD methods. **c** is the conversion from the diffraction rings to intensity versus d-spacing plot of **b**. **e** is the diffraction pattern of the starting material obtained by the EDXRD method. The diffraction peaks resolved in these patterns are shown as numbers and their corresponding d-spacings are listed in Table 1

Fig. 1a. The original two dimensional print-out of the diffraction patterns obtained by the image plate is shown in Fig. 1b, which was processed and shown as an ordinary diffractometric chart in Fig. 1c. The EDXRD pattern of the quenched $Al(OH)_3$ is shown in Fig. 1d. For comparison, the EDXRD pattern of the starting material is shown in Fig. 1e. The d-spacings corresponding to all of the 4 diffraction patterns in Fig. 1 are listed in Table 1 along with the peaks of gibbsite and nordstrandite according to the JCPDS cards. By comparing these diffraction peaks with those of gibbsite and nordstrandite, it is concluded that the diffraction patterns of the quenched sample can be interpreted as a mixture of both gibbsite and nordstrandite (Table 1).

Compressibility measurement

Figure 2 shows a series of the EDXRD spectra of $Al(OH)_3$ taken during the loading and unloading processes. At pressure lower than about 4 GPa, the X-ray patterns showed ten diffraction peaks of gibbsite, i.e., the (002), (110), (200), (20$\bar{2}$), (11$\bar{2}$), (21$\bar{1}$), ($\bar{1}$12), (31$\bar{1}$), (021) and (024). The d-spacings of these peaks decrease with pressure up to about 4 GPa. At 5.2 GPa, some new peaks started to show up and co-existed with those of gibbsite. The diffraction peaks of gibbsite disappeared

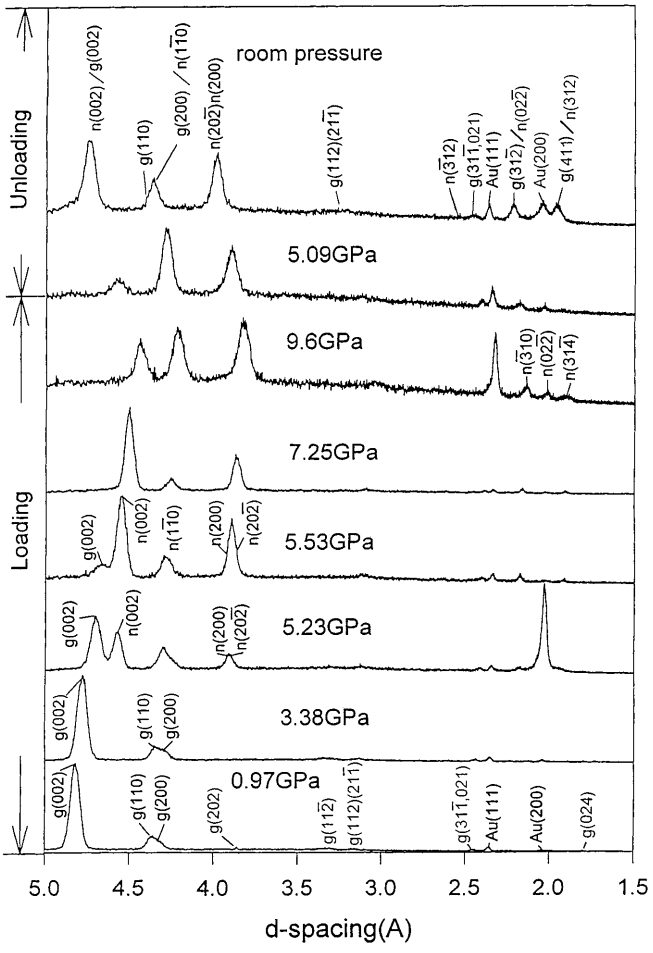

Fig. 2 A series of EDXRD patterns showing the phase transition in $Al(OH)_3$ with the increase (loading) and decrease (unloading) in pressure. Diffraction peaks of gibbsite and the high-pressure phase are denoted as *g* and *n*, respectively

Table 1 Comparison of the diffraction patterns of the starting material and the quenched sample of $Al(OH)_3$ with standard gibbsite and nordstrandite from the JCPDS cards[a]

Starting material		Quenched sample				Gibbsite			Nordstrandite		
EDXRD		EDXRD		IP	D-S	(hkl)	d (Å)	I/I_o	(hkl)	d (Å)	I/I_o
1	4.839 [7]	G/N	4.834 [6]	4.811 [26]	4.823 [s]	(002)	4.82	[100]	(002)	4.79	[100]
2	4.726 [5]	?	4.705 [10]	4.728 [60]	4.701 [m]	–	–	–	–	–	–
3	4.356 [38]	G/N	4.347 [30]	4.356 [100]	4.345 [s]	(110)	4.34	[40]	$(1\bar{1}0)$	4.33	[25]
4	–	G/N	–	–	4.242 [s]	(200)	4.30	[20]	(110)	4.22	[25]
5	–	N	3.959 [17]	3.978 [50]	4.011 [m]	–	–	–	(200)	4.16	[20]
6	–	N	–	–	3.885 [w]	$(20\bar{2})$	3.35	–	$(20\bar{2})$	3.896	[15]
7	3.328 [27]	G	3.319 [17]	3.324 [4]	3.330 [m]	$(11\bar{2})$	3.31	[6]	$(11\bar{2})$	3.604	[10]
8	3.184 [22]	G	3.188 [12]	3.200 [8]	3.210 [w]	$(21\bar{1},\bar{1}12)$	3.17	[8]	$(\bar{1}12)$	3.446	[10]
9	3.109 [100]	G	3.120 [7]	3.128 [3]	3.098 [w]	$(202,10\bar{3})$	3.08	[4]	$(1\bar{1}2)$	3.022	[15]
10	–	?	2.696 [3]	2.718 [3]	–	–	–	–	$(\bar{3}12)$	2.481	[15]
11	2.456 [65]	G/N	2.450 [100]	2.466 [30]	2.464 [s]	$(31\bar{1})$	2.44	[16]	$(3\bar{1}0)$	2.454	[10]
12	2.383 [72]	G/N	2.385 [40]	2.406 [12]	2.389 [m]	$(21\bar{3}, 311)$	2.37	[20]	(004, 310)	2.393	[35]
13	2.288 [11]	G/N	2.278 [19]	–	–	$(31\bar{2})$	2.28	[4]	$(02\bar{2})$	2.265	[35]
14	2.242 [10]	G	2.221 [47]	2.239 [27]	2.228 [s]	(022, 213)	2.23	[6]	–	–	–
15	2.162 [21]	G	2.160 [8]	2.189 [8]	2.191 [m]	(312)	2.15	[8]	–	–	–
16	2.051 [27]	G	2.051 [20]	2.068 [4]	2.050 [s]	$(204, 31\bar{3})$	2.03	[12]	–	–	–
17	1.994 [19]	G/N	1.975 [31]	1.990 [12]	1.965 [m]	(023)	1.98	[10]	$(\bar{3}14)$	2.015	[30]
18	1.917 [11]	G/N	1.910 [6]	–	1.876 [w]	(411)	1.90	[8]	$(31\bar{2})$	1.904	[20]
19	1.805 [15]	G/N	1.803 [9]	–	1.780 [w]	(314)	1.79	[10]	$(02\bar{4})$	1.781	[15]
20	1.751 [14]	G	1.749 [11]	1.746 [6]	1.723 [w]	$(02\bar{4})$	1.74	[10]	–	–	–
21	1.681 [9]	G	1.680 [5]	1.706 [2]	1.662 [w]	(323)	1.67	[10]	–	–	–
22	1.647 [4]	G	–	–	1.647 [w]	$(42\bar{0})$	1.65	[4]	–	–	–
23	–	G	1.634 [2]	1.623 [–]	1.628 [w]	$(42\bar{1})$	1.63	[2]	–	–	–
24	1.586 [5]	G/N	1.581 [5]	1.594 [3]	1.602 [w]	$(31\bar{5}, 42\bar{2})$	1.58	[4]	$(3\bar{1}6)$	1.595	[10]
25	–	N	1.499 [2]	1.513 [2]	1.503 [w]	–	–	–	$(3\bar{1}4)$	1.513	[10]
26	–	G/N	–	1.477 [8]	1.479 [m]	(–)	1.477	[2]	(602)	1.478	[10]
27	1.457 [9]	G	1.448 [15]	1.464 [14]	1.472 [m]	(–)	1.457	[3]	–	–	–
28	–	N	–	–	1.440 [w]	–	–	–	$(3\bar{3}0)$	1.440	[20]
29	1.440 [10]	G/N	–	1.432 [2]	1.420 [w]	(–)	1.441	[2]	(224)	1.431	[5]
30	1.410 [7]	G/N	1.407 [4]	1.405 [2]	1.408 [w]	(–)	1.409	[2]	(330)	1.403	[10]
31	–	?	–	1.306 [3]	1.312 [w]	–	–	–	–	–	–

[a] The unit for all d-spacings is in Å. *G* and *N* stand for gibbsite and nordstrandite, respectively. The numbers, xx, in [xx] indicate the relative intensity of the peak compared with the most intense peak in the pattern. In the film method, the intensity of the diffraction peaks is represented by letters: *s*, *m* and *w*, stand for strong, medium and weak, respectively

when the pressure was brought up to 5.5 GPa. Little change was observed when the sample was further compressed to a maximum pressure of 9.6 GPa. During the unloading process, the high-pressure phase persisted even at the ambient conditions.

During the loading process, the d-spacing of each diffraction peak can be calculated from the Ed value which was determined to be 71.14 KeV · Å at a fixed 2θ of 14°. The pressure of each run was determined from the equation of state of cold (Heinz and Jeanloz 1984) with its molar volume calculated based on the d-spacings of Au (111), (200), (220) and (311) peaks. The variation of d-spacing of each diffraction peaks versus pressure is shown in Fig. 3. The scheme for indexing the diffraction peaks above 4 GPa is discussed in the next section.

Discussion

Phase transformation in $Al(OH)_3$

It is clearly seen from the change in the diffraction patterns (Fig. 2) and the drastic change in the variation of d-spacing of each peak with pressure (Fig. 3) that a phase transformation in gibbsite has occurred above 4 GPa. In our previous EDXRD experiments carried out at the Photon Factory, Tsukuba, Japan, we also observed a phase transition took place (Huang et al. 1996). However, the exact pressure at which the phase transition occurred was not well defined because the pressure increment was too large (Huang et al. 1996). Subsequent Raman spectroscopic observation has revealed that gibbsite transforms to a high-pressure phase at 3 GPa (between 2.2 and 3.2 GPa; Huang et al. 1996). In the present EDXRD study, the phase transition was found to take place between 3.4 GPa and 5.2 GPa. This transition pressure is close to but still higher than that observed by the Raman spectroscopy. Since we have no data points between 3.4 and 5.2 GPa, the determination of the transition pressure relies on a comparison in relative intensity of the diffraction peaks between gibbsite and its HP phase. Judging from the relative intensity between n(002) and g(002) (Fig. 2), which represent the high-pressure and gibbsite phase, respectively, we think that the transition pressure should be much lower than 5.2 GPa where the HP phase has already reached its

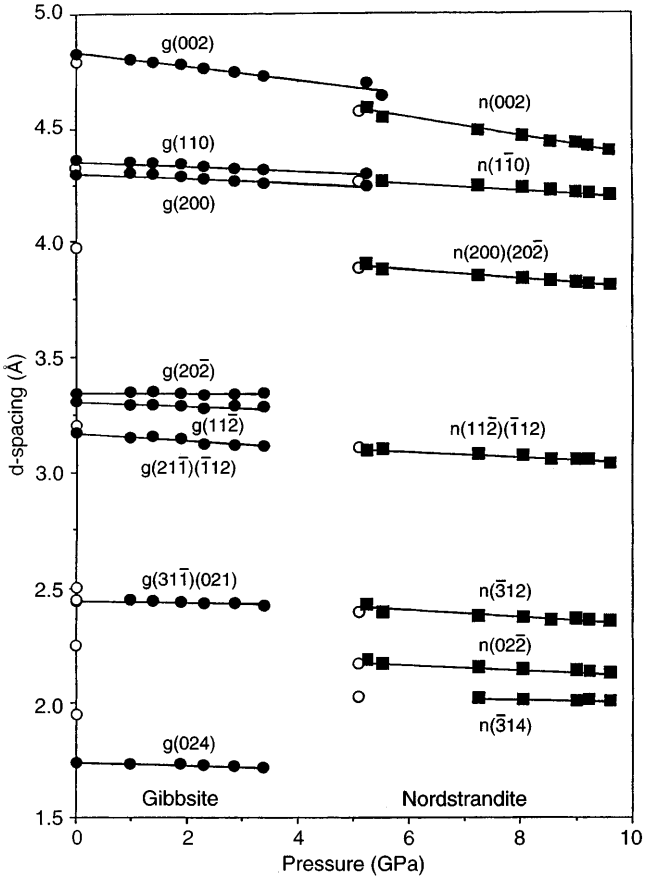

Fig. 3 The variations of d-spacings of all diffraction peaks with pressure. The phase transition is observed to take place between 3.4 and 5.2 GPa. The diffraction peaks are indexed and shown in the Figure. The *open circles* are the data taken during the unloading process

mature stage. However, even a lower value of 4 GPa is taken as the transition pressure, it still makes the value higher than that determined based on the Raman spectroscopic observation. Since the two polymorphs have very similar diffraction patterns but drastically different Raman spectra, it is likely that the structural change during the transition is not easily detected as the change in the vibrational modes (Huang et al. 1996). Therefore, the pressure at which transition occurs based on X-ray diffraction lags behind that of the Raman observation.

High-pressure phase of $Al(OH)_3$

The high-pressure phase of gibbsite has never been determined structurally in the past. From Figs. 1 and 2, it is clearly seen that the quenched phase is different from the starting material. Therefore, it is reasonable to check the diffraction patterns of the quenched phase with those of the polymorphs of $Al(OH)_3$. Although gibbsite has two other polymorphs, doyleite and bayerite, in addition to nordstrandite (Chao et al. 1985), we think the quenched HP phase of gibbsite fits best to nordstrandite. Among the 31 diffraction peaks detected in the quenched sample (Table 1), some of them are the diffraction peaks from the starting phase, gibbsite, and some of them can be interpreted as the mixture of both gibbsite and nordstrandite. The positive evidence for the presence of nordstrandite is provided by the diffraction peaks numbered as 5, 6, 25 and 28, which correspond to the (200), (20$\bar{2}$), (314) and (3$\bar{3}$0) of nordstrandite. The agreement in the value of d-spacing is in general within ± 0.005 Å, which is within the resolving power for image plate and EDXRD method. It is also in reasonable agreement with the film result despite the fact that some of the peaks show deviation in d-spacing that exceeds the uncertainty of the film method. However, since most of the diffraction peaks can be indexed as the mixture of gibbsite and nordstrandite, treating nordstrandite as the candidate for the HP phase of gibbsite is by no means fortuitous. It is noted that the relative intensity of the diffraction peaks of the quenched high-pressure phase are not fully in agreement with those of nordstrandite. The intensities of diffraction peaks of the material are affected by several factors such as the preferred orientation of the powdered sample, the interference of the coexisting phases, the intensity profile of the incident X-ray beam and the relaxation of the sample after being unloaded from the diamond cell. Therefore, the match in peak position should be a better criterion for correlating the diffraction peaks than relative intensity.

Further evidence that the HP phase is nordstrandite is found in high-pressure in situ compression experiments. Figure 4 shows the diffraction patterns of gibbsite obtained by the IP and EDXRD methods under a nominal pressure of 5 to 6 GPa. The diffraction pattern of gibbsite under a pressure of 5.5 GPa (using gold as pressure calibrant) is also shown in Fig. 4d for comparison. The patterns show clearly the (002), (1$\bar{1}$0), (200)/(20$\bar{2}$), (11$\bar{2}$)/($\bar{1}$12), ($\bar{3}$12), (02$\bar{2}$) and (31$\bar{4}$) diffraction peaks of nordstrandite. Although the relative intensity among these peaks is different, the peak positions match well with each other. Therefore, we conclude that the high-pressure phase of gibbsite is nordstrandite.

Compressibility measurements

The variations in the d-spacing of each diffraction line of gibbsite and its HP phase, nordstrandite, are shown in Fig. 3. Once the structure of both phases in $Al(OH)_3$ are identified, the variations of the cell parameters and molar volume with pressure of these phases can be determined. We have used the diffraction lines of (002), (110), (200), (20$\bar{2}$), (11$\bar{2}$), (21$\bar{1}$)/($\bar{1}$12), (31$\bar{1}$)/(021) and (024) for the determination of lattice parameters of gibbsite up to 5 GPa. For nordstrandite, the diffraction peaks of (002), (1$\bar{1}$0), (200)/(20$\bar{2}$), (11$\bar{2}$)/($\bar{1}$12), ($\bar{3}$12), (02$\bar{2}$) and ($\bar{3}$14) were used for the calculation of the lattice parameters of nordstrandite above 5 GPa. We have adopted the method of Novak and Colville (1989) for the calculation of the lattice parameters. The com-

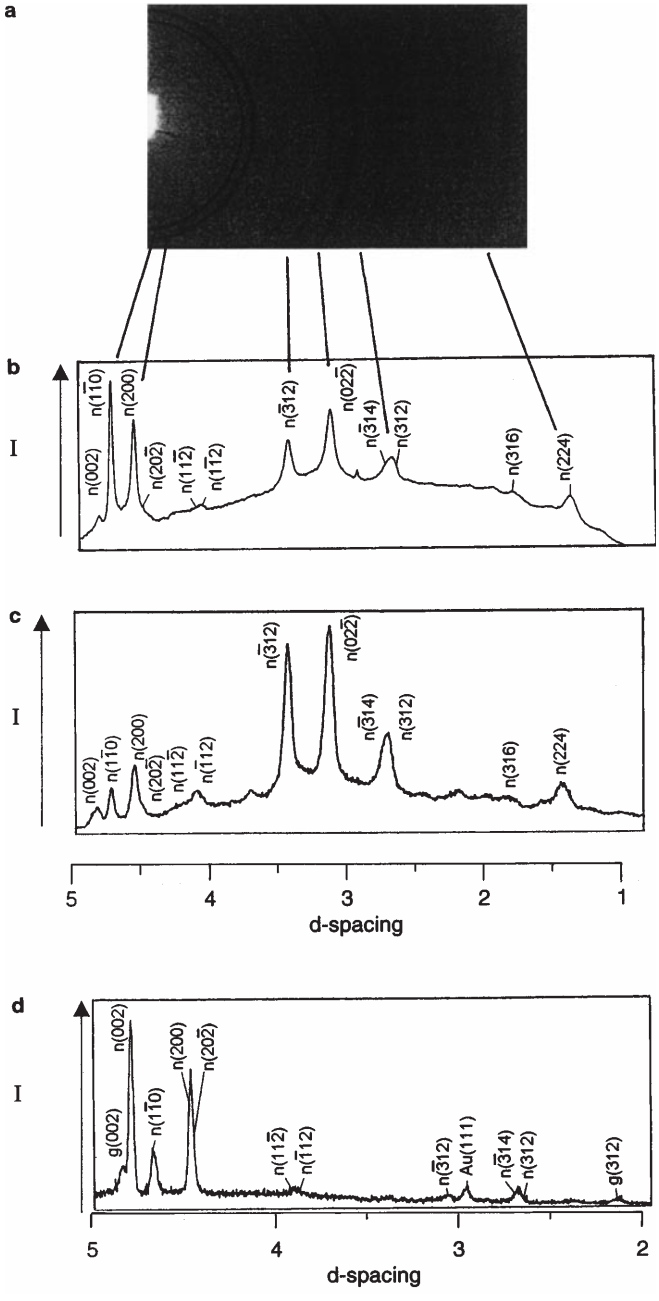

Fig. 4a–d The diffraction patterns of gibbsite obtained by **a** image plate at a nominal pressure of 6 GPa; **c** EDXRD method at a nominal pressure of 5 GPa; and **d** EDXRD method at 5.5 GPa. **b** is the conversion from the diffraction rings to intensity versus d-spacing plot of **a**. Note that **c** and **d** were taken at different 2θ angles

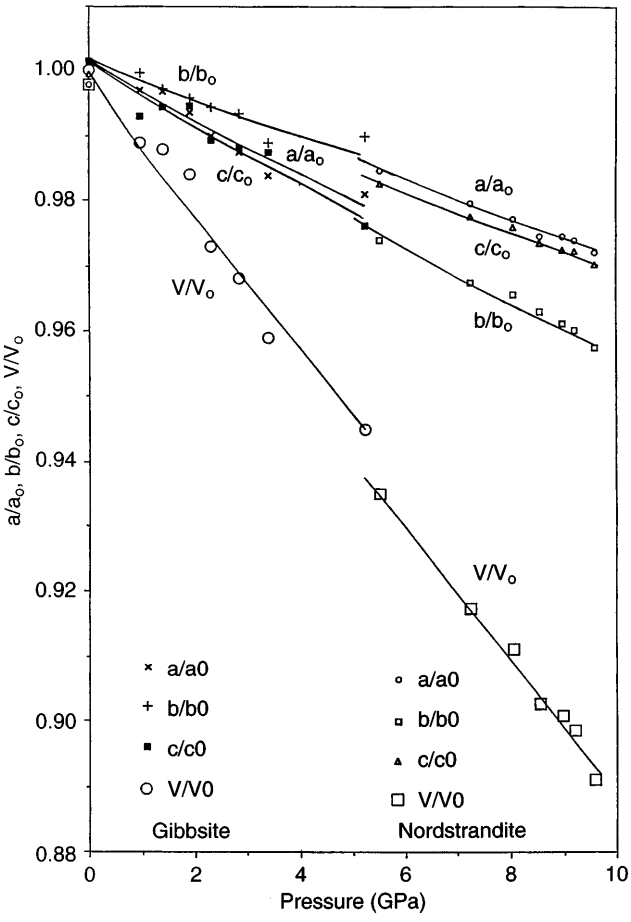

Fig. 5 The variations of a/a_o, b/b_o, c/c_o and V/V_o of two polymorphs of $Al(OH)_3$ with pressure. The molar volume compression curves represent a bulk modulus of 85 and 70 GPa for gibbsite and nordstrandite, respectively

pression data of these two phases are listed in Table 2 and plotted in Fig. 5. The bulk modulus of gibbsite and nordstrandite can be determined by fitting a Birch-Murnaghan equation of state to the data as 85 ± 5 GPa and 70 ± 5 GPa, respectively, assuming a first pressure derivative, K'_o, as 4 in both cases.

In gibbsite, the axial compressibility behaves as $c/c_o > a/a_o > b/b_o$ below 4 GPa. This is due to the dioctahedral sheets along the c axis, which are held by relatively weak hydrogen bonding, resulting in the largest compressibility along this direction (Fig. 6a). Along the a- and b-axis, the octahedral Al-$(OH)_6$ units link together by sharing edges and thus form stronger bonds than that along the c-axis. In nordstrandite, the axial compressibility is $b/b_o > c/c_o > a/a_o$, which can also be interpreted as due to the contribution of the hydrogen bonds along the b-axis while stronger bonds exist along the a- and c-axis where polyhedra are shared (Fig. 6b). The anisotropic compressibility is commonly observed in layered hydrous minerals in which bonds with non-uniform strength exist. Similar anisotropic compressibility is also found in diaspore (Xu et al. 1994). The present results also indicate that the compressibility of the high-pressure phase, nordstrandite, is slightly greater than that of its low-pressure phase, gibbsite.

The cell volume of the two phases of $Al(OH)_3$ can be calculated from their cell parameters since their structures are indentified. It is noted that the molar volume of nordstrandite (32.90 cm^3/mol) is slightly larger than that of gibbsite (31.48 cm^3/mol) at the ambient conditions (calculated from Table 2, with $Z = 8$). Therefore, it is expected that nordstrandite should be less stable than

Table 2 The compression data of two $Al(OH)_3$ polymorphs[a]

Gibbsite						Nordstrandite				
P(GPa)	a/a_0	b/b_0	c/c_o	β	V/V_o	P(GPa)	a/a_0	b/b_0	c/c_o	V/V_o
0	1.000	1.000	1.000	94.8	1.000	5.53	0.985	0.974	0.983	0.935
0.97	0.997	1.000	0.993	95.2	0.989	7.25	0.980	0.967	0.978	0.917
1.39	0.997	0.997	0.994	95.2	0.988	8.05	0.977	0.966	0.976	0.911
1.90	0.994	0.996	0.995	95.2	0.984	8.55	0.975	0.963	0.974	0.903
2.30	0.990	0.994	0.989	95.2	0.973	8.99	0.974	0.961	0.973	0.901
2.84	0.988	0.993	0.988	95.8	0.968	9.22	0.974	0.960	0.972	0.899
3.38	0.984	0.989	0.987	96.0	0.959	9.60	0.972	0.958	0.970	0.891
5.23	0.981	0.990	0.976	96.4	0.945	0	1.000	1.000	1.000	1.000

[a] The lattice parameters of gibbsite at room pressure are $a_o = 8.607$ Å, $b_o = 5.055$ Å, $c_o = 9.645$ Å and $\beta = 94.84°$, the unit cell volume $V_o = 418.1$ Å^3; those of nordstrandite are $a_o = 8.890$ Å, $b_o = 4.978$ Å, $c_o = 10.539$ Å and $\beta = 94.84°$, the unit cell volume$V_o = 437.2$ Å^3. Uncertainities in pressure reading, cell parameter ratio, beta angle and molar volume ratio are ±0.25 GPa, ±0.001, ±0.2° and ±0.003, respectively

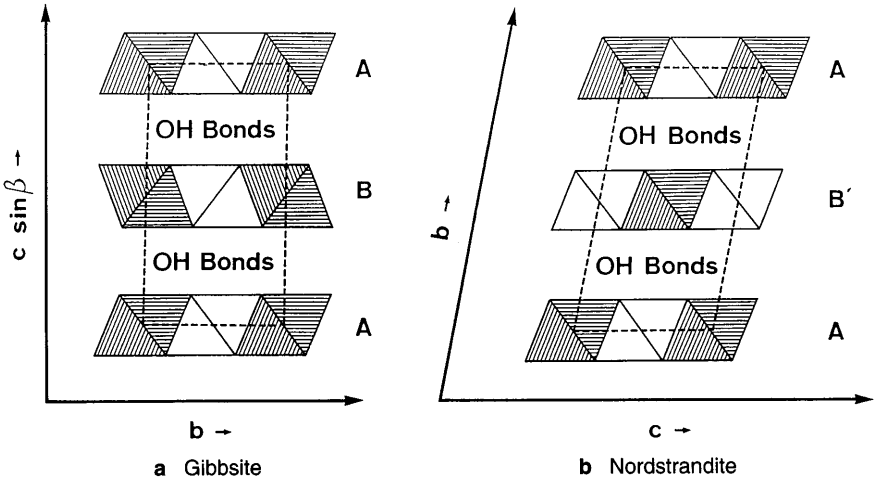

Fig. 6a, b The crystal structure of **a** gibbsite and **b** nordstrandite showing the arrangement of the polyhedral layers. The most compressible direction is along the *c*-axis and *b*-axis of gibbsite nordstrandite where the polyhedral layers are held by relatively weak hydrogen bonds (modified from Chao et al. 1985)

gibbsite at room pressure as pointed out by Schoen and Roberson (1970). In fact, gibbsite is the predominant $Al(OH)_3$ phase found in nature while nordstrandite is sporadically found in regions where the pH value is high (Schoen and Roberson 1970). However, when the variations of molar volume with pressure are compared for these two phases, it is interesting to see that nordstrandite has the same molar volume as gibbsite at about 2 GPa. As the pressure increases, the difference in molar volume between the gibbsite and its high-pressure polymorph becomes greater. Therefore, the phase transition from gibbsite to nordstrandite is thermodynamically favored above 2 GPa. Because the crystal structures of gibbsite and nordstrandite differ only in the stacking sequences of the dioctahedral sheets (Chao et al. 1985) and the molar volumes differ only slightly, it is likely that the high-pressure phase could be quenched at room pressure due to the difficulty in removing the remaining nordstrandite, during the process of regaining the atomic arrangement of the original phase. Epitaxial growth might have occurred during the phase transition when the two phases are structurally inter-related. The stress inherited during the initial growth of the HP phase in the matrix of low-pressure phase would cause the anomalous distortion in the lattice parameters of the HP phase (Bassett and Huang 1987). Therefore, it is likely that when nordstrandite was first produced from gibbsite, the lattice parameters would show anomalous distortion. However, the resolution of the present results is not good enough for the observation of this phenomenon. A detailed high-pressure single-crystal compression study on gibbsite would provide more information for the mechanism of the gibbsite-nordstrandite phase transition.

Acknowledgements The writers wish to express their thanks to the staff in the SRRC, CHESS and BNL for their persistent help during the experimental runs. We owe our thanks to Mr. Y.C. Yang, for his assistance in the computer programming work. This work was a follow-through of the discovery of Mr. Chen and Miss Li who had provided basic observations in high-pressure behavior of $Al(OH)_3$. This work was supported by the National Science Council, NSC 85-2111-M-001-021 and NSC 86-2613-M-213-015.

References

Akimoto S, Akaogi M (1984) Possible hydrous magnesian silicates in the mantle transition zone. In: Sunagawa I (ed) Material Science of the Earth's Interior. Terra Sci. Publ. Co., Tokyo, pp 477–480

Bassett WA, Huang E (1987) Mechanism of the body-centered cubic-hexagonal closed-packed phase transition in iron. Science 238: 780

Chao GY, Baker J, Sabina AP, Roberts AC (1985) Doyleite, a new polymorph of $Al(OH)_3$, and its relationship to bayerite, gibbsite and nordstrandite. Can Mineral 23: 21–85

Chen JH, Takemura K (1993) Two-dimensional angle-dispersive X-ray diffraction by an image plate with MAX80, 34th High-Pressure Conference. Rev High Pressure Sci Tech Spec Issue 2: 34–35

Desgranges L, Grebille D, Calvarin G, Chevrier G, Floquet N, Niepce JC (1993) Hydrogen thermal motion in calcium hydroxides: $Ca(OH)_2$. Acta Crystallogr B49: 812–817

Duffy TS, Meade C, Fei Y, Mao HK, Hemley RJ (1995) High-pressure phase transition in brucite, $Mg(OH)_2$. Am Mineral 80: 222–230

Heinz DL, Jeanloz R (1984) The equation of state of gold calibration standard. J Appl Phys 55: 885–893

Huang E (1996) Applications of Image Plate in high-pressure research (I): phase transitions in some dioxides. Report to National Science Council, R.O.C.

Huang E, Lin JF, Xu J, Yu SC (1995) Raman spectroscopic study of diaspore up to 25 GPa. J Geol Soc China 38: 25–36

Huang E, Li A, Xu J, Chen R, Yamanaka T (1996) High-pressure phase transition in $Al(OH)_3$: Raman and X-ray observations. Geophys Res Lett 23: 3083–3086

Johnson MC, Walker D (1993) Brucite [$Mg(OH)_2$] dehydration and the molar volume of H_2O to 15 GPa. Am Mineral 78: 271–284

Kirby SH (1987) Localized polymorphic phase transformations in high-pressure faults and applications to the physical mechanism of deep earthquakes. J Geophys Res 92: 13789–13800

Kruger MB, Williams Q, Jeanloz R (1989) Vibrational spectra of $Mg(OH)_2$ and $Ca(OH)_2$ under pressure. J Chem Phys 91: 5910–5915

Meade C, Jeanloz R (1990) Static compression of $Ca(OH)_2$ at room temperature: observations of amorphization and equation of state measurements to 10.7 GPa. Geophys Res Lett 17: 1157–1160

Meade C, Jeanloz R (1991) Deep-focus earthquakes and recycling of water into the Earth's mantle. Science 252: 68–72

Nelmes RJ, Hatton PD, McMahon MI, Piltz RO, Crain J, Cernik RJ, Bushnell-Wye G (1992) Angle-dispersive powder-diffraction techniques for crystal structure refinement at high pressure. Rev Sci Instrum 63: 1039–1042

Novak GA, Colville AA (1989) A practical interactive least-square cell-parameter program using an electronic spread-sheet and a personal computer. Am Mineral 74: 488–490

Pavese A, Catti M, Ferraris G, Hull S (1997) P-V equation of state of portlandite, $Ca(OH)_2$, from powder neutron diffraction data. Phys Chem Minerals 24: 85–89

Schoen R, Roberson CE (1970) Structures of aluminum hydroxide and geochemical implications. Am Mineral 55: 43–77

Shimomura O, Takemura K, Fujihisa H, Fujii Y, Ohishi Y, Kikegawa T, Amemiya Y, Matsushita T (1992) Application of an image plate to high-pressure x-ray study with a diamond anvil cell. Rev Sci Instrum 63: 967–973

Xia X, Weidner DJ, Zhao H (1998) Equation of state of brucite: single-crystal Brillouin spectroscopy study and polycrystalline pressure-volume-temperature measurement. Am Mineral 83: 68–74

Xu J, Hu J, Ming LC, Huang E, Xie H (1994) The compression of diaspore, AlO(OH) at room pressure up to 27 GPa. Geophys Res Lett 21: 161–164

Xu J, Huang E, Lin JF, Xu Y (1995) Raman study at high pressure and the thermodynamic properties of corundum: application to Kieffer's model. Am Mineral 80: 1159–1167